A Wearable All-Printed Textile-Based 6.78 MHz 15 W-Output Wireless Power Transfer System and its Screen-Printed Joule Heater Application

Mahmoud Wagih, *Member, IEEE*, Abiodun Komolafe, *Member, IEEE*, Irfan Ullah *Member, IEEE*, Alex S. Weddell, *Member, IEEE*, and Steve Beeby, *Fellow, IEEE*

***Abstract*—While research in passive flexible circuits for Wireless Power Transfer (WPT) such as coils and resonators continues to advance, limitations in their power handling and low efficiency have hindered the realization of efficient all-printed high-power wearable WPT receivers. Here, we propose a screen-printed textile-based 6.78 MHz resonant inductive WPT system using planar inductors with concealed metal-insulator-metal (MIM) tuning capacitors. A printed voltage doubler rectifier based on Silicon Carbide (SiC) diodes is designed and integrated with the coils, showing a power conversion efficiency of 80-90% for 2-40 W inputs over a wide load range. Compared to prior wearable WPT receivers, it offers an order of magnitude improvement in power handling along with higher efficiency (approaching 60%), while using all-printed passives and a compact rectifier. The coils exhibit a simulated Specific Absorption Rate (SAR) under 0.4 W/kg for 25 W received power, and under 21°C increase in the coils' temperature for a 15 W DC output. Additional fabric shielding is investigated, reducing harmonics emissions by up to 17 dB. We finally demonstrate a wirelessly-powered textile-based carbon-silver Joule heater, capable of reaching up to 60°C at 2 cm separation from the transmitter, as a wearable application which can only be wireless-powered using the proposed system.**

***Index Terms*—Antennas, Coils, Heaters, Inductors, Rectifiers, Resistors, RFID, Wireless Power Transfer.**

I. Introduction

FLEXIBLE wearable systems represent the closest sensing and actuation platform to the user [1]. Emerging wearable sensing systems [2]–[4], antennas [5], and body area networks [6] have mostly been implemented using flexible or textile-based materials, for seamless integration into clothing. It is widely recognized that conventional batteries are not a wearable-friendly option [1], [7]–[9], leading to research efforts seeking a solution in wireless power transfer (WPT) [9]–[12] and in flexible or wearable energy harvesters [7], [13].

While low-power wearable sensors can be powered using far/mid-field WPT [14], wearable applications such as Joule heaters [15] or mobile neural network classification processors, sampling wearable sensors [16], cannot be powered using any of the reported wearable textile-based energy harvesting or WPT solutions. To explain, wearable mid/far-field WPT solutions are focused on µW to mW applications [9], [17], [18]. Moreover, wearable and implantable near-field WPT research is mostly focused on the passive electromagnetic link [11], [19]–[21], with no flexible or textile-based rectifiers designed and optimized for wearable or large-area electronics.

Individual additively-manufactured passive components, however, show promise for all-printed WPT receivers. For example, inkjet printed RLC circuits have been reported on smooth thin films, handling around 100 mW [22]. Furthermore, printed capacitors on rough textile substrates have recently been demonstrated with better microwave power-handling (up to 1 W) than their discrete ceramic counterparts [23]. Printed textile-based coils were integrated with rigid FR4-based Qi-standard circuitry in [24] and demonstrated receiving around 1.5 W with a 37% DC-DC efficiency. In [25], we demonstrated a 3.75 W 6.78 MHz WPT receiver based on a flexible rectifier and resonant embroidered coils. However the WPT system in [25] had several limitations which cannot be solved using existing flexible and wearable WPT implementations including: (a) low power-handling capability of compact (<1 cm) surface-mount tuning capacitors, (b) low efficiency of the rectifier due to the high switching speed and the small form-factor, (c) high thermal losses with a peak temperature exceeding 200°C, and (d) unreliable packaging due to using multiple fabrication processes (embroidered coils, copper-based rectifier), and the surface mismatch caused by the flexible-rigid interface between the tuning rigid capacitors and the coils. Therefore, there has been no work to date demonstrating the feasibility of efficient (>50%) and high-power (>3 W) WPT using all-flexible resonators and power conversion circuits.

In this paper, we propose a printed textile-based wirelessly-powered system which addresses the outstanding challenge

Manuscript received Month xx, 2xxx; revised Month xx, xxxx; accepted Month x, xxxx. This work was supported by the UK Engineering and Physical Sciences Research Council (EPSRC) under Grant EP/P010164/1, the European Commission through the EnABLES Project grant number: 730957. The work of M. Wagih was supported by the UK Royal Academy of Engineering (RAEng) and the Office of the Chief Science Adviser for National Security under the UK Intelligence Community Post-Doctoral Research Fellowship programme. The work of S. Beeby was supported by the RAEng under the Chairs in Emerging Technologies scheme. (*Corresponding author: Mahmoud Wagih*).

M. Wagih is with the James Watt School of Engineering, the University of Glasgow, Glasgow, G12 8QQ, U.K. (phone: +44 0141 330 5042, email: mahmoud.wagih@glasgow.ac.uk).

A. Komolafe, A. S. Weddell, and S. Beeby are with the School of Electronics and Computer science, University of Southampton, Southampton, SO17 1BJ, U.K. (email: aok1g15; asw; spb@ecs.soton.ac.uk)

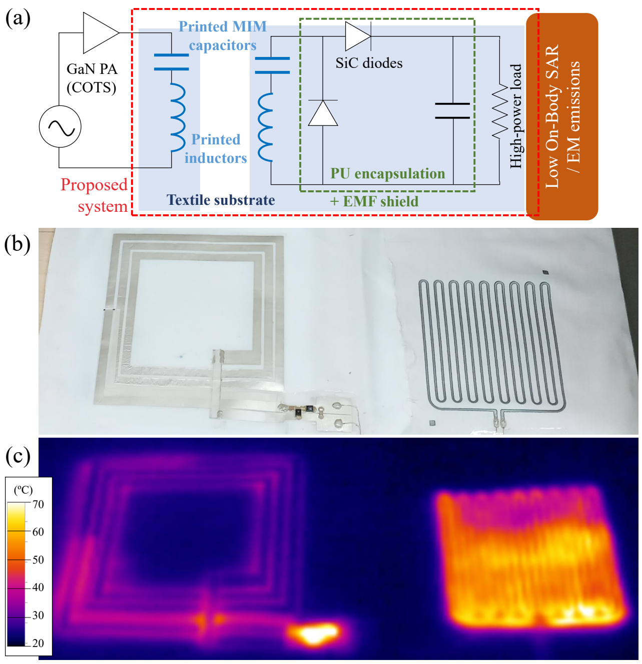

Fig. 1. Overview of the proposed high-power wearable WPT: (a) High-level schematic of the system; (b) photograph of the integrated system; (c) thermal image showing the system's operation.

of high-power wearable WPT, that is the realization of an all-flexible WPT receiver. First, the design and fabrication of screen-printable resonant coils, suitable for integration on any textile substrate is presented (Section II), achieving up to 70% link efficiency (Section III). The coils are integrated with a flexible textile-based >90%-efficient voltage doubler, using off-the-shelf diodes, receiving over 14 W with an end-to-end efficiency of 60% (Section IV-A and B), and is demonstrated powering a printed heater with over 2 cm range (Section IV-C).

II. All-Printed Coils Design and Fabrication

To enable textile-integrated WPT to supply high-power wearable applications, such as the Joule heater presented here, the system illustrated in Fig. 1 is proposed. A typical printed e-textile heater consumes over 1 W of DC power [15], implying that existing wearable WPT systems cannot power these directly and must instead charge a battery which in turn periodically supplies the textile heater.

The coils and their tuning capacitors are realized using an inexpensive screen printing and lamination process, detailed in the next section, enabling them to achieve higher power handling than prior work utilizing discrete components [25]. The rectifier is seamlessly integrated on the same textile substrate and encapsulated for mechanical reliability. Both textile-based and conventional transmitter coils are characterized, using small-signal s-parameters, investigating the potential for WPT transmitters being integrated in non-wearable and industrial textiles used in furnishings (e.g.s chairs). Fig. 1(b) and (c) show the complete system being wirelessly-powered using a textile-based transmitting coil, placed beneath the visible coil in the photograph, driven by a Commercial-Off-The-Shelf (COTS) GaN power amplifier (PA) demonstration kit (GSWP050W-EVBPA).

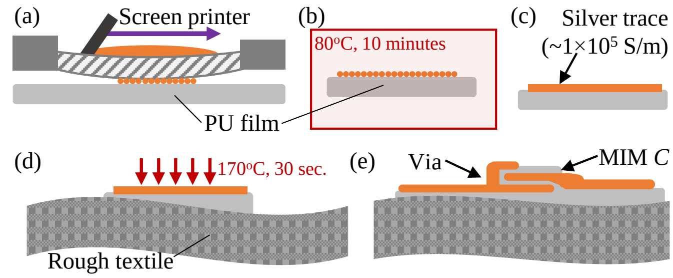

Fig. 2. Fabrication steps of the textile-based coils: (a) printing the conductors on the transfer layer; (b) initial curing; (c) the dried silver adhesive (PU)-backed film; (d) heat-transfer onto a textile substrate ; (e) the assembled structure.

A. Fabrication Method and Material Characterization

Instead of directly screen printing on the substrate, e.g. rough fabrics, the conductors are printed on a smooth 75 µm-thick polyurethane (PU) film, which is then heat-pressed onto the fabric, as in Fig. 2(a) to (d). To explain, fabric typically requires blanket coated textiles or the prior screen printing of specialist interface layers [26], and can limit curing temperatures. We have previously shown that by printing on the PU film, the printed traces can withstand over 10,000 bending cycles and can be applied to different textiles regardless of their roughness [23]. For WPT applications at kHz frequencies, printed coils could be fabricated with Litz-like geometries using the same process [27].

By laminating multiple PU/silver layers onto the textile, metal-insulator-metal (MIM) capacitors can be realized, as in Fig. 2(e), which can be used to tune the coils. These capacitors exhibit improved mechanical reliability over their inkjet counterparts [22], [28], which are restricted to smooth polymers and thin conductors. The large-area printed capacitors can achieve higher power handling than discrete ceramic capacitors. Once the circuit is printed, the components are attached using conductive epoxy, cured at 90°C, then encapsulated using a PU superstrate for mechanical reliability.

Following the calculation [29] or measurement of the printed coils' inductance, detailed in Section II-B, the tuning capacitor can be integrated on the same substrate. To realize tuning capacitors C for resonant WPT, C is given by

$$C = \frac{1}{4\pi^2 f_r^2 L} = \epsilon_{\mathrm{PU}} \frac{W_c L_c}{t} \quad (1)$$

where f_r=6.78 MHz, ϵ_{PU} is the permittivity of the PU film at 6.78 MHz, in Fig. 3, t=55 µm, the measured height of the heat-pressed dielectric, with L_c and W_c representing the length and width of the integrated tuning capacitor, respectively, as shown in Fig. 5(a).

The relative permittivity of the heat-pressed PU laminates was measured using a test MIM capacitor of known dimensions. The capacitance was measured using a Wayne Kerr 6500 impedance analyzer between 100 Hz and 10 MHz, which

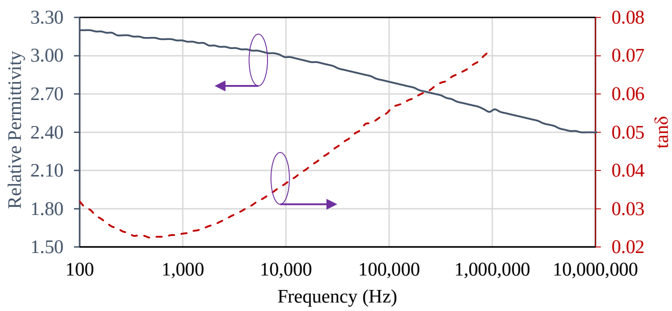

Fig. 3. Measured real relative permittivity and tanδ of the 55 µm-thick pressed PU with silver conductors.

is lower than the capacitor's self-resonant frequency (SRF). Fig. 3 shows the calculated $\Re\{\epsilon_r\}$ of the PU laminate, where it can be seen that the PU maintains $\Re\{\epsilon_r\}$=2.4 at 6.78 MHz.

B. Coil, Capacitor, and Rectifier Design

Four square coils of varying sizes were designed. The inductance of the coils was approximated using the modifier Wheeler formula by Mohan *et al.* for printed inductors [29]. The uniform square geometry was chosen due to its simple closed-form analysis [30] and its wide adoption in flexible and printed electronics [31]. Table I summarizes the geometrical and electrical parameters of each coil, along with their measured inductance; the layout of a 3-turn (n=3) coil is shown in Fig. 5(a), where the laminated capacitor can be observed. In a 1:1 WPT link, the mutual inductance L_M between planar coils could be calculated using the solution to the Neumann's integral for the current over the coils, by Raju *et al.* [30] as

$$L_M = \frac{\mu}{4\pi} \oint_{C_{TX}} \oint_{C_{RX}} \frac{\mathrm{d}l_{TX}\mathrm{d}l_{RX}}{s}, \tag{2}$$

over the coil's surface. The total L_M can be expressed as

$$L_M = \rho \times \sum_{i=n_{TX}}^{i=1} \sum_{j=n_{RX}}^{j=1} M_{ij} \tag{3}$$

$$L_{M,ij} = \frac{\mu_0 \pi a_i^2 b_j^2}{2(a_i^2 + b_j^2 + d^2)} (1 + \frac{15}{32}\gamma_{ij}^2 + \frac{315}{1024}\gamma_{ij}^4) \tag{4}$$

$$a_i = b_i = D/2 - (n_i - 1)(w + s); \ \rho = \frac{4}{\pi^2} \tag{5}$$

with d being the separation between the coils.

Along with the printed coils and tuning capacitors, a flexible textile-based rectifier is integrated on the same substrate. The rectifier is a voltage doubler based on a Silicon Carbide (SiC) Schottky diode (GB01SLT12-214). This diode was chosen due to its low resistance and capacitance enabling a high RF to DC power conversion efficiency (PCE) and low thermal losses. Moreover, the diodes have a reverse break-down voltage of 1.2 kV. It was observed in [25] that a rectifier based on Silicon diodes with higher series resistance and 600 V breakdown voltage resulted in a PCE under 40%, and a temperature exceeding 200°C, limiting the power handling. A voltage doubler topology was chosen to enable a high voltage output that could, for example, directly power a wearable heater (as detailed later) without DC-DC conversion, as well as to

TABLE I
SUMMARY OF THE COILS' PARAMETERS

Coil	Calc. L (µH)	Meas. L, 6.78 MHz	Meas. R, 6.78 MHz	w (mm)	s (mm)	D (mm)	n
A	1.40	1.60 µH	5.2 Ω	10	2.5	150	3
B	1.71	1.56 µH	6.4 Ω	5	2.5	120	3
C	1.98	2.03 µH	9.5 Ω	2.5	2.5	105	3

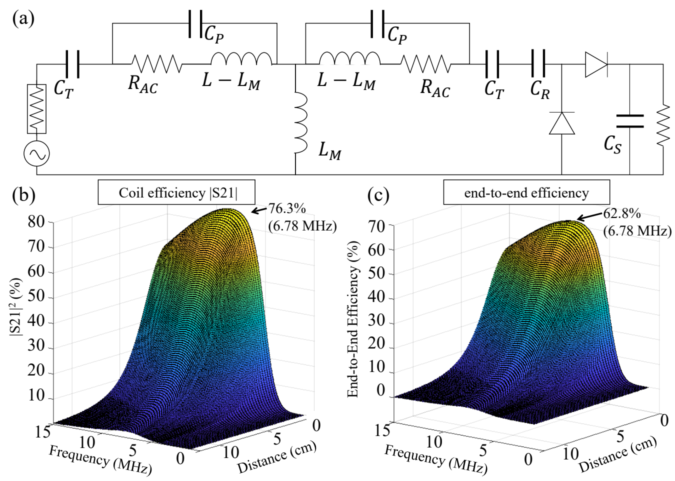

Fig. 4. (a) equivalent circuit model of the WPT system (b) analytical link efficiency over frequency and separation; (c) end-to-end efficiency as a function of frequency and separation.

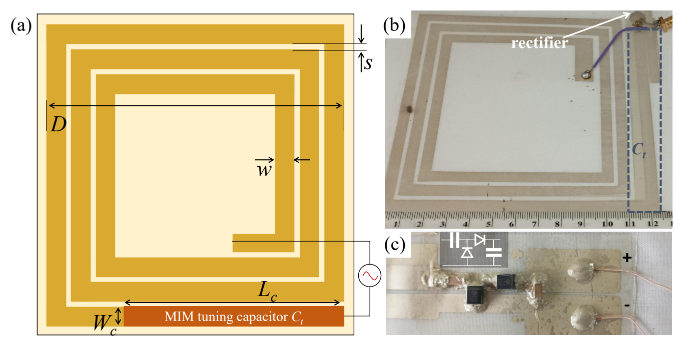

Fig. 5. (a) Generic layout of the coils showing the key dimensions; (b) photograph of coil A; (c) schematic and photograph of the rectifier showing the encapsulation and coils interface.

reduce the component count. This reduces the packaging and layout complexity and overall cost, improving the system's robustness. The simulated and measured DC output of the rectifier is presented in Section IV-A-A.

Using the calculated L_M, an equivalent circuit model combining the coupling of the coils and the rectifier based can be constructed [10], as shown in Fig. 4(a). The coupling efficiency of the coils was analytically calculated as the $|S_{21}|^2$ of the circuit, assuming the rectifier is replaced with an ideal 50 Ω load for varying d and frequency and is shown in Fig. 4(b), for L=1.41 µH, R_AC=5.4 Ω, representing coil A from Table I. For the maximum coupling between the coils, i.e. at minimum separation, the circuit parameters in Fig. 4(a) are C_T=393 pF, $R_{AC} = 4 + f^{1.36}/1 \times 10^{-10}\Omega$, C_P=10 pF, $(L - L_M)$=0.52 µH, L_M=1.09 µH, C_R=1 nF, C_S=1 nF. The AC resistance was obtained using the fitted frequencydependence of the printed silver, where the high-frequency resistance increases due to the surface roughness of the inks; the supplementary material show the equivalent circuit model parameters for all fabricated coils. The diodes' model was based on the datasheet parameters.

The small-signal coil efficiency was calculated based on the equivalent circuit model and is shown in Fig. 4(b), for varying separation and frequency. To calculate the end-to-end efficiency of the system, non-linear harmonic balance simulation was used to calculate the rectifier's efficiency, with the amplifier's efficiency assumed to be 90%, as an average of its large-signal efficiency based on the vendor's datasheet. The end-to-end efficiency was calculated as $\eta = \eta_{PA} \times |S_{21}^2 \times \eta_{rect.}(P)$, where the rectifier's efficiency $\eta_{rect.}$ is a function of the input power, due to the rectifier's non-linearity. This is reflected in the closed-form calculation using a curve-fitter function, made available in the article's dataset. The rectifier's efficiency is assumed to be constant over frequency, as it varies by under 3% in the non-linear simulation. Fig. 4(c) shows the calculated large-signal end-to-end efficiency, for an input power level exceeding 10 W.

While the diode used is not flexible or printable, existing solution-processed Schottky diodes cannot support the required power levels beyond 1 W [32]. The flexibility of the circuit can be improved by using a bare-die component on a thinned chip, making it more bendable [33], where the reliable integration of bare-dies within e-textiles has previously been demonstrated [34]. The rectifier was encapsulated using a conformable pressed PU film, improving the mechanical reliability and isolating the conductive traces from the user.

III. Small-Signal Coil and Link Characterization

The coil parameters were measured using the VNA from 1 to 10 MHz, and are shown in Fig. 6. The calculated response of the fitted equivalent circuit model are shown alongside the measured response; the equivalent circuit model's parameters are shown in the paper's supplementary material. The coil parameters are compared to the analytical L in Table I. A Rohde & Schwarz ZVB4 Vector Network Analyzer (VNA) was used to measure the s-parameters of the coils under varying separation and misalignment. SMA connectors were added to the resonant coils with the concealed capacitors to interface with the VNA, as shown in Fig. 5(b). The measured Q-factor (under 5 around 6.78 MHz) is comparable to previously reported printed coils implemented on smooth films [22], [35], showing that printing on the PU first and then laminating on to the textile does not affect coil properties.

The s-parameters of the one-to-one link, based on the printed coils, were simulated in CST Microwave Studio and measured using the VNA. Fig. 7 shows the simulated and measured s-parameters of the one-to-one link based on coils A and C, in close agreement. The conductivity of the coils was modelled as σ=1$\times$10^4 S/m. From the S_{11} response, it can be seen that the coils are matched ($S_{11} < -10$ dB) for separations under 2 cm, which is attributed to their relatively low inductance.

The s-parameters of the printed WPT coils were then characterized with a standard wire coil representing a non-

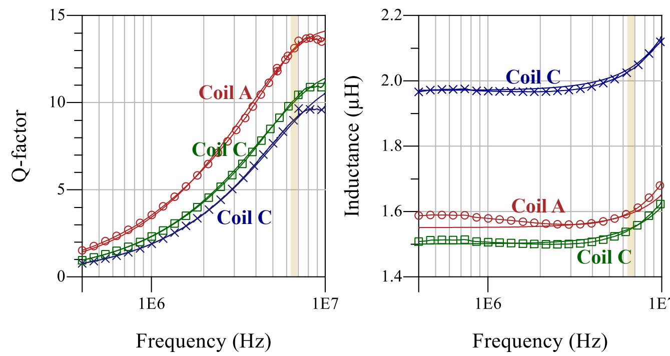

Fig. 6. Measured (markers) and calculated (solid line, no markers) equivalent circuit model's broadband inductance and Q-factor of the printed coils before integrating the tuning capacitors.

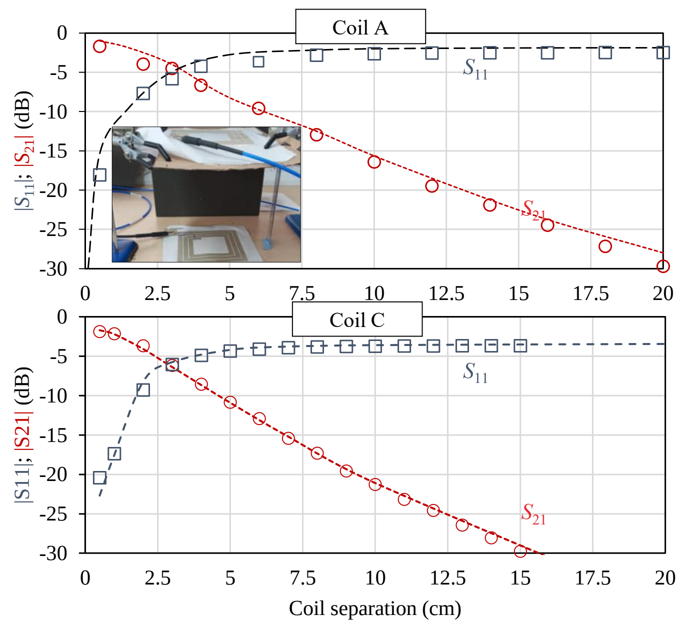

Fig. 7. Simulated (dashed line) and measured (solid markers) s-parameters of the symmetric link using coils A and C over varying distance; the inset shows the measurement setup.

textile transmitter. The coil is fabricated using a stranded wire of 1.5 mm^2 area, to act as a reference transmitter coil. The wire coil is composed of 5 turns, D=15 cm and has an inductance of 5.2 μH inductance, and 70 mΩ series resistance at 6.78 MHz. The forward transmission (S_{21}) between textile-based coils and the Litz coil was characterized for varying vertical separation as well as lateral misalignment. Fig. 8 shows the measured S_{21} as a function of vertical separation. To investigate the influence of the printed capacitor on the link, the s-parameters of coil C were also measured with a discrete ceramic tuning capacitor alongside the printed capacitor.

From Fig. 8, it can be seen that there is minimal influence on the S_{21} from using the printed capacitor. Moreover, the S_{21} variation with vertical separation is directly linked to the coil's radius, which is attributed to the effect of the gap on the mutual inductance [30]. Frequency-splitting and over-coupling [10] are not observed due to their relatively low Q-factor of the coils. The effect of lateral misalignment on the S_{21},

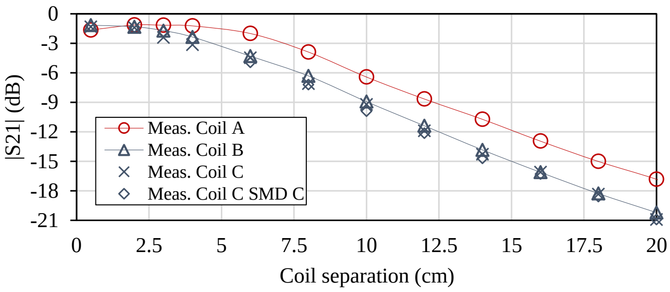

Fig. 8. Measured forward transmission between the textile coils and the reference wire transmitter over varying coil separations.

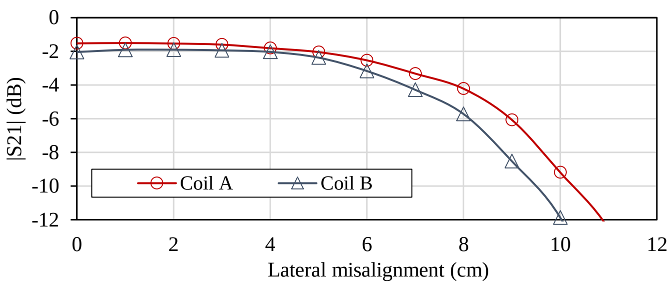

Fig. 9. Measured forward transmission between the textile coils and the reference wire transmitter over varying coil misalignments.

shown in Fig. 9, is directly related the coils' radii and the relative misalignment between the transmitting and receiving coil areas.

It is noted that the use of different coil geometries [36] or intermediate resonant coils or "meta-surfaces" can improve the link efficiency [11], [37]. However, the main focus of this work is to demonstrate a high-power WPT-enabled wearable system using all-printed passives, which to date has primarily been hindered by the rectifiers' or resonators' power handling as opposed to efficient resonator design.

IV. High-Power WPT Characterization

A. Rectifier Simulation and Measurements

The rectifier was simulated in Keysight ADS using harmonic balance simulation. The diode's parameters were taken from the datasheet and the 1 nF charge-pumping and smoothing capacitors were assumed to be ideal. A connectorized prototype of the proposed rectifier was fabricated for experimental validation. A load sweep was performed to identify the optimum load impedance Z_L in the >1 W power range; the rectifier maintains over 90% of its peak RF-DC efficiency for Z_L between 250 and 300 Ω. To characterize the rectifier under high power levels, the rectifier was connected directly to the 50 W PA demonstration kit's output and the PA's supply voltage was varied.

The input RF power was calculated using the PA's datasheet peak efficiency of 91% for a conservative estimate of the rectifier's performance. Fig. 10 shows the simulated and measured DC output and efficiency of the rectifier for varying RF inputs up to the PA's maximum output. Despite its flexible and low-cost implementation, the rectifier can generate up to 35 W

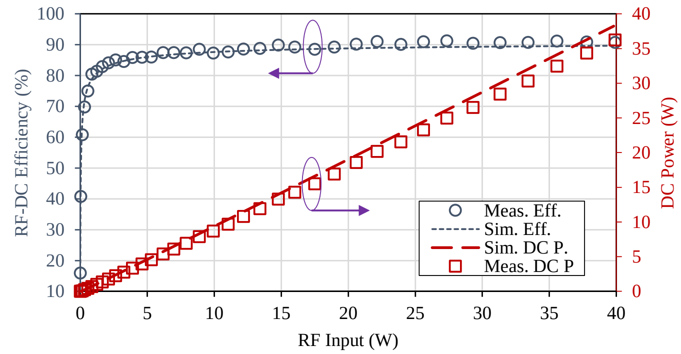

Fig. 10. Simulated and measured PCE and DC voltage output of the rectifier across a 261 Ω load.

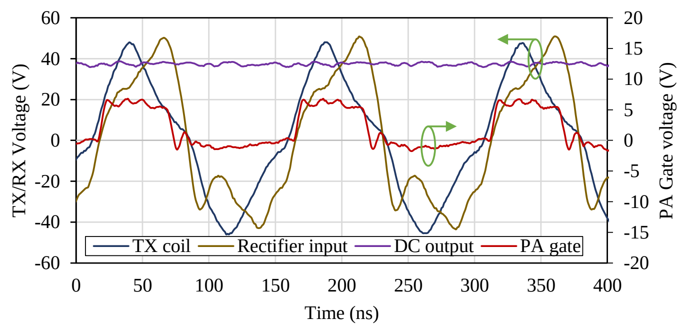

Fig. 11. Time-domain waveforms across the gate driver, transmitting and receiving coils, and the load.

DC output with an efficiency over 80% for inputs exceeding 1 W. This represents over 20× improvement over previously reported WPT rectifiers reported for wearable (Qi) applications [24], where the system's output was limited to 1.51 W, or operating at higher frequencies for near-field charging of textile-based devices [17].

B. Coil and System Characterization

The rectifier's layout was integrated with the MIM capacitor and the screen-printed coils on a single substrate, as seen in Fig. 1(b). Coil A (having the largest dimensions and Q-factor) was used to characterize the full WPT system. Two identical coils were used for transmitting and receiving, thereby enabling the power handling ability of the textile coil to be investigated.. The separation between the two coils has been kept under 5 mm, formed by the textile substrates and a non-uniform air gap due to the coils' flexibility. In this configuration, the coils maintained an S_{21}=−1.7 dB translating to a WPT link efficiency of 67%. Combined with the rectifier's efficiency of approximately 90% and the PA's DC-RF efficiency exceeding 91%, an end-to-end efficiency between 55% and 60% could be expected depending on the PA and rectifier's power-dependent performance. Fig. 11 shows the time-domain voltage waveforms across the coils, the gate driver, and the load, when the coils are approximately 1 cm apart driven at 10 W DC input.

To evaluate the system's power handling, the DC input to the PA was varied for a fixed coil separation of approximately 5 mm. Fig. 12 shows the measured end-to-end system effi-

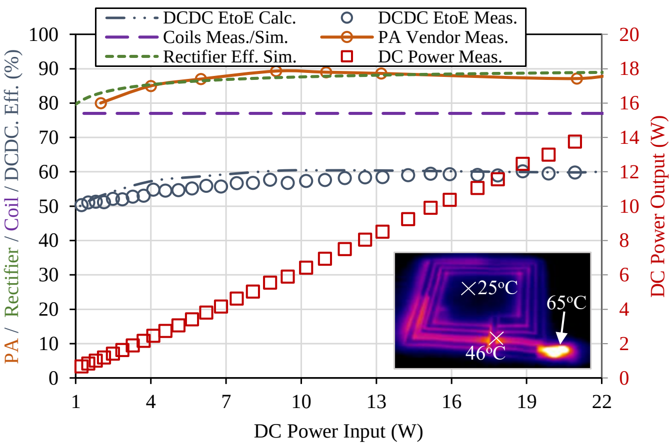

Fig. 12. Measured DC output of a small gap (<0.5 cm) wireless gap, the end-to-end DC-DC efficiency, and a break-down of the individual component efficiencies as a function of the DC input; the inset shows the system's temperature when driven at 22 W.

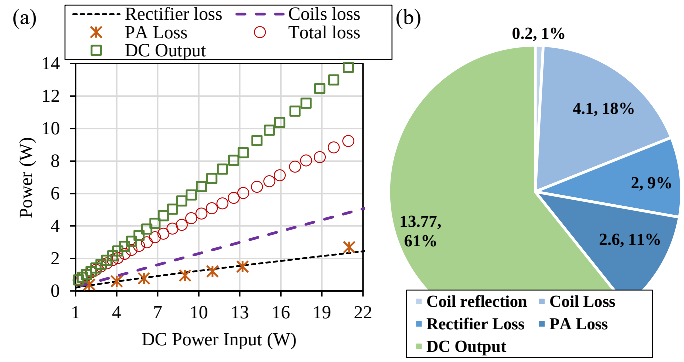

Fig. 13. Power loss analysis: (a) the measured DC output and the simulated/calculated losses at each stage for varying DC inputs; (b) the measured losses for Fig. 12 when driven at 22 W.

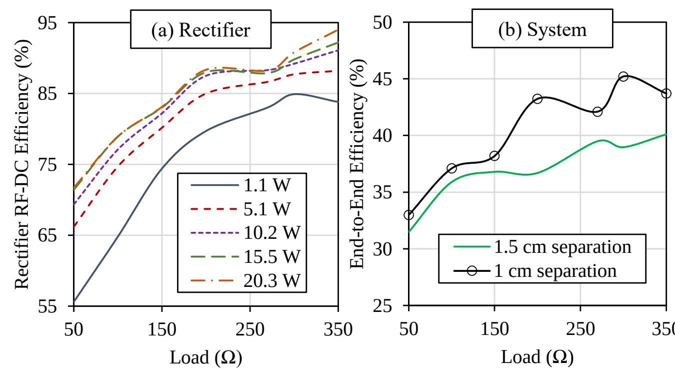

Fig. 14. Effect of varying load impedances on the efficiency: (a) RF-DC rectifier efficiency; (b) end-to-end WPT efficiency.

ciency and the DC power delivered to the load as a function of the DC input. The end-to-end efficiency was also calculated using the coils' simulated efficiency (assumed to be linear and is in close agreement with the measurements as in Fig. 7), the rectifier's simulated efficiency, and the PA's datasheet efficiency measured by the vendor. Both the calculated and measured DC-DC end-to-end efficiencies are shown in Fig. 12, showing a close agreement and indicating that the coils (due to their series resistance) have the lowest efficiency in the system. The maximum DC input of 21 W was limited by the PA's current draw at maximum bias, which could be further increased through adaptive impedance matching or using multiple loads. However, as this work focuses on the coil, power conversion, and load implementation, such optimizations were not explored.

From Fig. 12, it can be seen that the maximum expected efficiency of 60% is approached for high input power levels, and that the end-to-end efficiency exceeds 50% for inputs exceeding 1.5 W. At its maximum DC power output of 14 W, a 60 V potential was measured across the 261 Ω 100 W-rated dummy load. To explore the coils' power handling, an infrared (IR) thermal camera (Testo 875i) was used to observe the temperature over the receiving coil.

The inset in Fig. 12 shows the peak temperatures measured over the receiving coil's surface while being driven at a 21 W DC input, where a maximum temperature rise of 21°C is observed over the coil, and around 40°C rise is recorded at the rectifier. The higher temperature increase over the rectifier's surface is attributed to the diodes' series resistance being confined to their very small footprint, resulting in lower heat dissipation. However, the proposed rectifier and tuning capacitor reduce the temperature rise over prior flexible rectifiers, which could not operate above 4 W due to the temperature rising above 180 °C [25]. The observed peak temperature of 65° falls within the diodes' specified operation range and is also lower than the curing temperature of the printed silver traces, implying no damage to either component. The system was driven at 22 W for over five minutes with no noticeable change in the voltage waveforms or the temperature profile.

The power losses in the system have been quantified using both the calculations and the measurements. In Fig. 13(a), the power losses at each stage are shown based on the analytical coil efficiency calculations, and based on the SPICE-simulated rectifier circuit; the PA efficiency was based on the vendor-measured values from the datasheet. Fig. 13(b) shows the breakdown of the measured losses for the direct link used to evaluate the system's power handling and end-to-end efficiency. The coil reflection was estimated based on the full-wave simulated and measured small-signal S_{11} of the coils, around −20 dB.

Both the end-to-end efficiency and the rectifier's RF-DC efficiency were characterised for varying loads at different power levels, and are shown in Fig. 14(a) and (b), respectively. From the measured efficiency response, it can be seen that the load can be varied across a 7:1 resistance ratio, enabling high-current loads to be powered. The observed fluctuations in Fig. 15(b) are attributed to minor fluctuations in the coils' separation, which are more noticeable at shorter ranges.

Given the system's wearable application, minimising spurious emissions is essential. The electromagnetic fields around the receiving coil and its integrated rectifier were measured using a near-field probe (Rohde and Schwarz RS.H 400-1), connected to the oscilloscope. The Fast Fourier Transform (FFT) is shown in Fig. 15. The fields were measured around the coil's turns, away from the rectifier, and directly above the

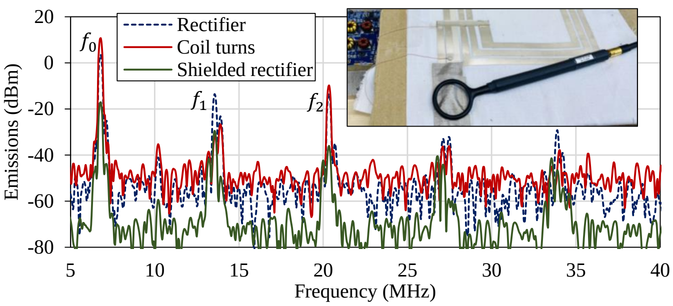

Fig. 15. Measured frequency-domain response of the receiving coil showing the fundamental (6.78 MHz) tone and its harmonics; the inset shows the measurement setup of the shielded rectifier

diodes. Due to their non-linearity, the rectifying diodes are expected to generate additional harmonics. From Fig. 15, it can be seen that the second and third harmonics are around −11 dBm over the rectifier. To demonstrate the feasibility of shielding the proposed rectifier, a layer of conductive fabric was attached to the encapsulating PU layer. As observed in Fig. 15, the additional shielding layer reduces the first- and second-order harmonics by up to 17 dB, to under −20 dBm. Additional magnetic shielding could also be used based on flexible ferrite films.

C. Wireless-Powered Heater System Evaluation

A key example of thermal e-textiles are long-term therapeutics and recovery [15], [38], where a temperature up to 60°C could be required. The performance of the WPT system if further evaluated in conjunction with the load, the resistive printed heater. To realize the heater on the same fabric substrate, a 65%/35% carbon/silver paste was prepared and screen-printed onto a PU film which is then laminated on the same textile material alongside the coils. The carbon/silver formula was optimized to achieve a resistance as close as possible to the optimum load of the rectifier. The heater is formed of a meandered trace with 18 folds and is 9×9 cm. The cured and laminated heater had a measured low-voltage resistance of 270 Ω at room temperature. Fig. 16(a) shows the experimental setup used in evaluating the wireless-powered heater.

Prior to testing the integrated system, the heater was connected directly to a bench DC power supply to evaluate its power requirements. The IR camera was used to observe the thermal distribution over the heater and a thermocouple was placed where the highest temperatures were observed to cross-validate the IR measurements. Fig. 17 shows the heater's temperature change and absolute peak temperate as a function of its DC input up to 30 V. In most wearable rehabilitation and treatment applications, temperatures exceeding 60°C are not typically required [39]. Therefore, the maximum DC power consumption of the heater can be estimated to be 3 W.

The heater was subsequently connected to the rectifier's output, as in Fig. 16(a), and a DC input power sweep was performed at two different separations between the transmitting and receiving textile coils. Low resistance conductive copper threads were used to connect the rectifier's DC output to the heater to demonstrate that the heater could be placed on a different body part to that hosting the coil. Fig. 18 shows the measured DC power delivered to the heater and the calculated end-to-end efficiency of the WPT system as it powers the load. The temperature of the wearable heater when driven at 15 W is shown in the IR photographs in Fig. 16(b) to (d), including when the heater is bent.

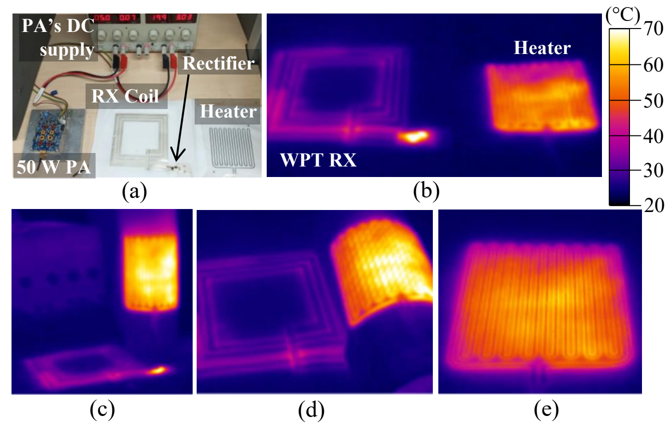

Fig. 16. The wireless-powered heater: (a) measurement setup the transmitting coil is placed beneath the identical receiver and connected to the PA with a low-loss coaxial cable); (b) IR image under flat conditions (<0.5 cm coil separation); (c, d) the functional heater under bending; (e) the heater powered with a 2 cm gap between the coils with a 3 W DC received power.

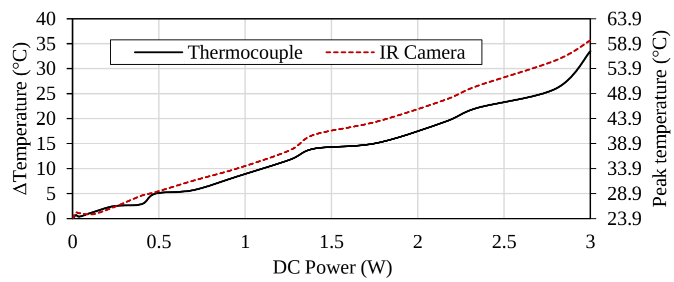

Fig. 17. Peak temperature of the screen-printed carbon/silver heater using a bench power supply.

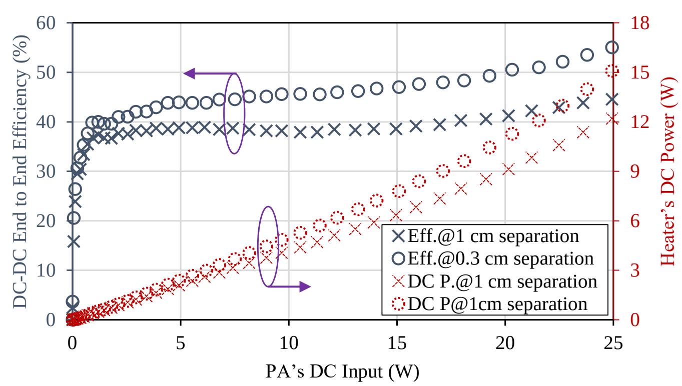

Fig. 18. The end-to-end efficiency and received power using the heater as a load for varying input power levels at different separations.

It can be observed in Fig. 18 that the peak end-to-end efficiency approaches that observed with the dummy resistive load. Moreover, a peak DC power output of 15 W could be

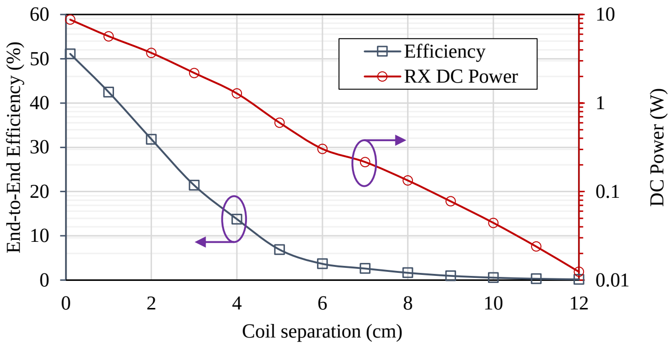

Fig. 19. Characterization of the DC power delivery to the heater over varying separation from the transmitter.

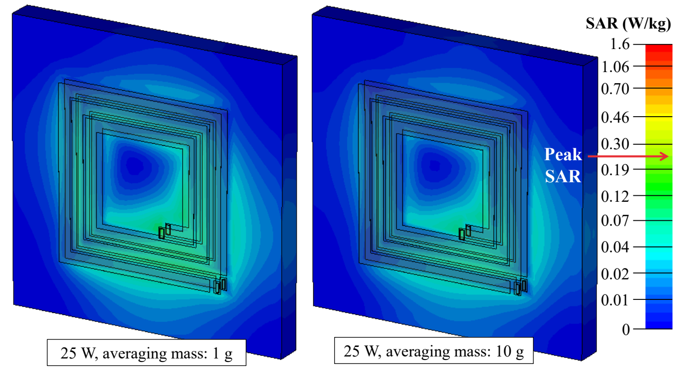

Fig. 20. Simulated SAR distribution for 25 W of 6.78 MHz power at the receiving (on-body) coil.

delivered to the heating element. Given the maximum power consumption of 3 W for a peak temperature of 59°C to be reached by the heater, in Fig. 18, the received DC power is sufficient for powering multiple heating elements on different body parts. The control circuitry could also be powered within the available energy budget and a wearable energy storage device could also be charged [9].

Following the validation of the WPT-powered heating system and identifying 3 W as the peak power consumption of the individual heater, the system was characterized for varying coil separations. Fig. 19 shows the measured DC power output as a function of the distance between the textile-based transmitter and receiver. At 2 cm separation, the DC power output is just over 3 W which can supply the heater with an end-to-end efficiency around 30%; this efficiency is comparable to that of a Qi-standard WPT system which can only deliver 1.2 W with minimal coil separation and using rigid power conversion circuitry of higher complexity [24]. The observed drop in the efficiency for varying separation is attributed to the impedance mismatch at the PA's output. This can be mitigated through the use of an adaptive matching network [40] on the transmitter, which does not need to be flexible or textile-based. The transmitter coil could also be driven at a constant current to achieve load-independent operation [41].

In Fig. 16(e), the temperature across the surface of the heater with the 2 cm coil separation results in a peak temperature exceeding 60°C. At higher separation distances, the power output drops to mW levels which can only be used to power smaller sensors and wearable devices. Beyond 12 cm, the DC power output is comparable to that of radiative far-field WPT systems implying that a dual-mode near/far-field implementation could be utilized [18], [25].

The final step in characterizing the WPT system is evaluating its safety for use in a standard unregulated setting. The Specific Absorption Rate (SAR) was simulated over a homogeneous skin phantom placed with 1 mm separation from the receiving coil. The SAR was calculated in CST Microwave Studio and averaged over 10 and 1 g tissue mass. Fig. 20 shows the simulated SAR distribution, calculated for a 25 W input at the on-body receiving coil. With a peak SAR of 0.247 W/kg for a 25 W received RF power level, it can be seen that the coils operate well below the 1.6 W/kg SAR limit of the IEEE C95.1 standard. Therefore, the main limiting factor for

TABLE II
COMPARISON WITH RECENT WEARABLE WIRELESS POWER RECEIVERS

Work and WPT mode	DC Power	Peak Efficiency	Resonator/ antenna material	Rectifier materials
This work: IPT	1–15 W with >50% DC-DC efficiency	DC-DC: 60%; RF-DC: 90%	Printed silver on textile	Printed silver with SiC diodes
[24]: Qi IPT	1.51 W with <37% DC-DC efficiency	DC-DC: 37%; RF-DC: NR	Screen-printed coil	COTS Qi rectifier
[25]: 6.78 MHz resonant IPT	1–3.5 W with <32% DC-DC efficiency	DC-DC: 32%; RF-DC: ≈45%	Embroidered e-thread	Discrete capacitor with Si diodes
[17]: E/H mid-field coupling	1–200 mW	DC-DC: <5%; RF-DC: 50-80%	Embroidered e-thread	Discrete matching with Si diodes
[9]: far-field radiation	0.1–20 mW	DC-DC: <0.1%; RF-DC: 50-80%	Flexible circuit filament in textile	Discrete matching and diodes on a flex filament

NR: not reported, off-the-shelf rectifier

the power level at which the coils can be driven at will be the heat dissipation of both the coils and rectifier, which could cause discomfort to the user.

Despite the extensive literature on electromagnetic near-field links for wearable WPT, there are limited works which have demonstrated a full system including the power conversion circuitry and a load. Table II compares this work to state-of-the-art wearable WPT receivers from the near-field to far-field. From Table II, it can be seen that the proposed system represents over a five-fold improvement in the DC power output over previous flexible WPT implementations and at least 100% DC-DC efficiency improvement, while being the first to use an all-flexible receiver. Moreover, the all-flexible screen-printed fabrication process enables the system to be scaled for most large-area industrial electronic applications. Finally, this work is the first to demonstrate a high-power wearable application, a textile-based Joule heater, being wirelessly-powered using COTS semiconductors and printed textile-based passives with a high DC-DC efficiency approaching that of a dummy load.

V. Conclusion

This paper presented an all-flexible printable WPT system and demonstrated it powering a textile-based Joule heater on the same substrate. The designed voltage doubler maintains an RF-DC efficiency over 80% for >1 W inputs, and a peak efficiency over 90% up to 40 W. The integrated system demonstrated a DC-DC efficiency approaching 60% with a 14 W DC output, enabling the textile-based heater to be powered at 2 cm away from the transmitter. The proposed system overcomes the limitations of existing flexible and wearable WPT systems based on:

1) High power handling: achieved through embedding a large-area low-loss tuning capacitor within the coil for improved thermal dissipation.
2) Reduced thermal losses: achieved through the use of low-loss diodes, reducing the temperature rise by nearly three-fold over previous flexible rectifiers.
3) Improved application-specific end-to-end efficiency, achieved by designing the load (the heating element) to approach the optimum current draw of the rectifier for improved RF-DC conversion.
4) Improved reliability and printability: by limiting the use of discrete rigid components to the SiC diodes as well as fabricating and encapsulating all passives using the same screen-printing process.

This work shows for the first time that flexible e-textile WPT systems can deliver Watt-level outputs efficiently. The printed heater demonstrated evidences that high-power wearable applications could become battery-free using WPT.

Acknowledgment

Datasets supporting this article will be made available from DOI: 10.5525/gla.researchdata.1432.

References

[1] M. Wagih, L. Balocchi *et al.*, "Microwave-enabled wearables: Underpinning technologies, integration platforms, and next-generation roadmap," *IEEE Journal of Microwaves*, vol. 3, DOI 10.1109/JMW.2022.3223254, no. 1, pp. 193–226, 2023.

[2] H.-T. Chang and J.-Y. Chang, "Sensor glove based on novel inertial sensor fusion control algorithm for 3-d real-time hand gestures measurements," *IEEE Transactions on Industrial Electronics*, vol. 67, DOI 10.1109/TIE.2019.2912765, no. 1, pp. 658–666, 2020.

[3] D. Patron, W. Mongan *et al.*, "On the use of knitted antennas and inductively coupled rfid tags for wearable applications," *IEEE Transactions on Biomedical Circuits and Systems*, vol. 10, DOI 10.1109/TBCAS.2016.2518871, no. 6, pp. 1047–1057, 2016.

[4] B.-J. Kim, Y. Jang *et al.*, "Self-powered carbon nanotube yarn for acceleration sensor application," *IEEE Transactions on Industrial Electronics*, vol. 68, DOI 10.1109/TIE.2020.2977541, no. 3, pp. 2676–2683, 2021.

[5] R. Pei, M. P. Leach *et al.*, "Wearable ebg-backed belt antenna for smart on-body applications," *IEEE Transactions on Industrial Informatics*, vol. 16, DOI 10.1109/TII.2020.2983064, no. 11, pp. 7177–7189, 2020.

[6] X. Tian, P. M. Lee *et al.*, "Wireless body sensor networks based on metamaterial textiles," *Nature Electronics*, vol. 2, pp. 243–251, 2019.

[7] L. Costanzo, M. Liu *et al.*, "Backpack energy harvesting system with maximum power point tracking capability," *IEEE Transactions on Industrial Electronics*, vol. 69, DOI 10.1109/TIE.2021.3053896, no. 1, pp. 506–516, 2022.

[8] A. Komolafe, B. Zaghari *et al.*, "E-textile technology reviewâfrom materials to application," *IEEE Access*, vol. 9, DOI 10.1109/ACCESS.2021.3094303, pp. 97 152–97 179, 2021.

[9] M. Wagih, N. Hillier *et al.*, "Rf-powered wearable energy harvesting and storage module based on e-textile coplanar waveguide rectenna and supercapacitor," *IEEE Open Journal of Antennas and Propagation*, vol. 2, DOI 10.1109/OJAP.2021.3059501, pp. 302 – 314, 2021.

[10] T. Imura and Y. Hori, "Maximizing air gap and efficiency of magnetic resonant coupling for wireless power transfer using equivalent circuit and neumann formula," *IEEE Transactions on Industrial Electronics*, vol. 58, no. 10, pp. 4746 – 4752, 2011.

[11] L. Li, H. Liu *et al.*, "Efficient wireless power transfer system integrating with metasurface for biological applications," *IEEE Transactions on Industrial Electronics*, vol. 65, DOI 10.1109/TIE.2017.2756580, no. 4, pp. 3230–3239, 2018.

[12] V. Pecunia, S. R. P. Silva *et al.*, "Roadmap on energy harvesting materials," *Journal of Physics: Materials*, 2023. [Online]. Available: http://iopscience.iop.org/article/10.1088/2515-7639/acc550

[13] S. Lemey, F. Declercq, and H. Rogier, "Textile Antennas as Hybrid Energy-Harvesting Platforms," *Proc. IEEE*, vol. 102, no. 11, pp. 1833 – 1857, 2014.

[14] Z. Liu, P. Wu, and G. Li, "A multibeam and surface plasmonic clothing with rf energy-localized harvester for powering battery-free wireless sensor," *IEEE Internet of Things Journal*, vol. 9, DOI 10.1109/JIOT.2022.3142781, no. 15, pp. 13 955–13 964, 2022.

[15] Q. Liu, B. Tian *et al.*, "Recent advances in printed flexible heaters for portable and wearable thermal management," *Materials Horizons*, vol. 8, DOI 10.1039/D0MH01950J, no. 6, p. 1634â1656, Jun. 2021. [Online]. Available: https://pubs.rsc.org/en/content/articlelanding/2021/mh/d0mh01950j

[16] Y. Tang, L. Zhang *et al.*, "Multi-scale deep feature learning for human activity recognition using wearable sensors," *IEEE Transactions on Industrial Electronics*, DOI 10.1109/TIE.2022.3161812, pp. 1–1, 2022.

[17] D. Vital, P. Gaire *et al.*, "An ergonomic wireless charging system for integration with daily life activities," *IEEE Transactions on Microwave Theory and Techniques*, vol. 69, DOI 10.1109/TMTT.2020.3029530, no. 1, p. 947â954, Jan. 2021.

[18] M. Wagih, A. Komolafe *et al.*, "Broadband compact substrate-independent textile wearable antenna for simultaneous near- and far-field wireless power transmission," *IEEE Open Journal of Antennas and Propagation*, vol. 3, DOI 10.1109/OJAP.2022.3167089, pp. 398–411, 2022.

[19] S. H. Kang and C. W. Jung, "Textile Resonators With Thin Copper Wire for Wearable MR-WPT System, year=2017," *IEEE Microwave and Wireless Components Letters*, vol. 27, DOI 10.1109/LMWC.2016.2629976, no. 1, pp. 91–93.

[20] S. H. Kang, V. T. Nguyen, and C. W. Jung, "Analysis of mrâwpt using planar textile resonators for wearable applications," *IET Microwaves, Antennas & Propagation*, vol. 10, DOI 10.1049/iet-map.2016.0024, no. 14, p. 1541â1546, Nov. 2016. [Online]. Available: https://onlinelibrary.wiley.com/doi/10.1049/iet-map.2016.0024

[21] M. Wagih, A. Komolafe, and B. Zaghari, "Dual-Receiver Wearable 6.78 MHz Resonant Inductive Wireless Power Transfer Glove Using Embroidered Textile Coils," *IEEE Access*, vol. 8, pp. 24 630 – 24 642, 2020.

[22] A. E. Ostfeld, I. Deckman *et al.*, "Screen printed passive components for flexible power electronics," *Sci. Rep.*, vol. 5, DOI 10.1038/srep15959, p. 15959, 2015.

[23] M. Wagih, A. Komolafe, and N. Hillier, "Screen-printable flexible textile-based ultra-broadband millimeter-wave dc-blocking transmission lines based on microstrip-embedded printed capacitors," *IEEE Journal of Microwaves*, vol. 2, DOI 10.1109/JMW.2021.3126927, no. 1, pp. 162–173, 2022.

[24] Y. Li, N. Grabham *et al.*, "Textile-Based Flexible Coils for Wireless Inductive Power Transmission," *Applied Sciences*, vol. 8, DOI 10.3390/app8060912, no. 6, 2018.

[25] M. Wagih, A. Komolafe *et al.*, "1 μw-3.75 w dual-mode near/far-field wearable wireless power transfer using a hybrid rectenna," in *2022 Wireless Power Week (WPW)*, DOI 10.1109/WPW54272.2022.9853859, pp. 298–301, 2022.

[26] K. Yang, R. Torah *et al.*, "Waterproof and durable screen printed silver conductive tracks on textiles," *Textile Research Journal*, vol. 83, pp. 2023 – 2031, 2013.

[27] I. Lope, C. Carretero *et al.*, "Frequency-dependent resistance of planar coils in printed circuit board with litz structure," *IEEE Transactions on Magnetics*, vol. 50, DOI 10.1109/TMAG.2014.2337836, no. 12, pp. 1–9, 2014.

[28] B. S. Cook, J. R. Cooper, and M. M. Tentzeris, "Multi-layer rf capacitors on flexible substrates utilizing inkjet printed dielectric poly-

mers," *IEEE Microwave and Wireless Components Letters*, vol. 23, DOI 10.1109/LMWC.2013.2264658, no. 7, pp. 353–355, 2013.

[29] S. Mohan, M. del Mar Hershenson *et al.*, "Simple accurate expressions for planar spiral inductances," *IEEE Journal of Solid-State Circuits*, vol. 34, DOI 10.1109/4.792620, no. 10, pp. 1419–1424, 1999.

[30] S. Raju, R. Wu *et al.*, "Modeling of mutual coupling between planar inductors in wireless power applications," *IEEE Transactions on Power Electronics*, vol. 29, no. 1, pp. 481 – 490, 2014.

[31] K. Pan, Y. Fan *et al.*, "Sustainable production of highly conductive multilayer graphene ink for wireless connectivity and iot applications," *Nature Communications*, vol. 9, DOI 10.1038/s41467-018-07632-w, no. 1, p. 5197, Dec. 2018. [Online]. Available: https://www.nature.com/articles/s41467-018-07632-w

[32] J. Semple, D. G. Georgiadou *et al.*, "Flexible diodes for radio frequency (RF) electronics: a materials perspective," *Semiconductor Science and Technology*, vol. 32, 2017.

[33] C. Hoyer, L. Steinweg *et al.*, "Bendable 190-ghz transmitter on 20-Î¼m ultra-thin sige bicmos," *IEEE Journal on Flexible Electronics*, vol. 1, DOI 10.1109/JFLEX.2022.3167372, no. 2, pp. 122–133, 2022.

[34] M. Li, J. Tudor *et al.*, "Novel Electronic Packaging Method for Functional Electronic Textiles," *IEEE Trans. Components, Packaging and Manufacturing Technology*, vol. 9, no. 2, pp. 216 – 225, 2019.

[35] B. S. Cook, C. Mariotti *et al.*, "Inkjet-printed, vertically-integrated, high-performance inductors and transformers on flexible LCP substrate," in *2014 IEEE MTT-S International Microwave Symposium (IMS2014)*, DOI 10.1109/MWSYM.2014.6848575, pp. 1–4, 2014.

[36] M. R. Basar, M. Y. Ahmad *et al.*, "An improved wearable resonant wireless power transfer system for biomedical capsule endoscope," *IEEE Transactions on Industrial Electronics*, vol. 65, DOI 10.1109/TIE.2018.2801781, no. 10, pp. 7772–7781, 2018.

[37] S.-J. Huang, T.-S. Lee *et al.*, "Intermediate coil-aided wireless charging via interactive power transmitting with misalignment-tolerating considerations," *IEEE Transactions on Industrial Electronics*, vol. 69, DOI 10.1109/TIE.2021.3123665, no. 10, pp. 9972–9983, 2022.

[38] J. T. Selsby and S. L. Dodd, "Heat treatment reduces oxidative stress and protects muscle mass during immobilization," *American Journal of Physiology-Regulatory, Integrative and Comparative Physiology*, vol. 289, DOI 10.1152/ajpregu.00497.2004, no. 1, p. R134âR139, Jul. 2005. [Online]. Available: https://journals.physiology.org/doi/full/10.1152/ajpregu.00497.2004

[39] H. McGorm, L. A. Roberts *et al.*, "Turning up the heat: An evaluation of the evidence for heating to promote exercise recovery, muscle rehabilitation and adaptation," *Sports Medicine*, vol. 48, DOI 10.1007/s40279-018-0876-6, no. 6, p. 1311â1328, Jun. 2018. [Online]. Available: https://doi.org/10.1007/s40279-018-0876-6

[40] S. Jeong, T.-H. Lin, and M. M. Tentzeris, "A real-time range-adaptive impedance matching utilizing a machine learning strategy based on neural networks for wireless power transfer systems," *IEEE Transactions on Microwave Theory and Techniques*, vol. 67, DOI 10.1109/TMTT.2019.2938753, no. 12, pp. 5340–5347, 2019.

[41] S. Aldhaher, D. C. Yates, and P. D. Mitcheson, "Load-independent class e/ef inverters and rectifiers for mhz-switching applications," *IEEE Transactions on Power Electronics*, vol. 33, DOI 10.1109/TPEL.2018.2813760, no. 10, p. 8270â8287, Oct. 2018.

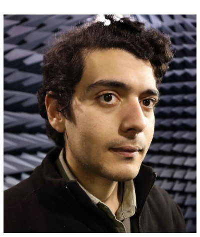

Mahmoud Wagih (GS'18, M'21) received his B.Eng. (Hons.) in September 2018, and his Ph.D. on rectenna design in April 2021, both in Electrical and Electronic Engineering from the University of Southampton.

He is currently a UK Intelligence Community Research Fellow and Proleptic Lecturer (Assistant Professor) at the University of Glasgow. His interests broadly cover RF and antenna-enabled sustainable electronics including energy harvesting, sensing, and wearable applications.

Dr. Wagih was the recipient of 15+ awards including the "EurAAP" Per-Simon Kildal Award for the Best PhD in Antennas and Propagation and the Best in Engineering and Physical Sciences Doctoral Research Award at the University of Southampton, Best Student Paper Prize at IEEE WPTC 2019, Best Three Minutes Thesis (2nd Place) at the IEEE Microwave Week, 2020, the Best Paper at PowerMEMS (IEEE) in both 2019 and 2021, and the URSI Young Scientist Award in 2022. He is a Senior Member of URSI, an affiliate member of the IEEE Microwave Theory & Technologies (MTT) Technical Committees TC-25, on Wireless Power, and a member of IEEE MTT TC-26, on RFID, Wireless Sensors, and IoT.

Abiodun Komolafe received the B.Sc. degree (Hons.) in physics from the University of Ibadan, Nigeria, in 2007, the M.Sc. degree in microelectromechanical systems, in 2011, and the Ph.D. degree in printed circuits on fabrics from the University of Southampton, in 2016.

He currently works as a Research Fellow with the University of Southampton in investigating novel manufacturing methods for making functional electronics on textiles using flexible electronic circuits and screen-printed electronics for medical applications. He is experienced in the design and fabrication of e-textiles using screen printing and thin-film technologies

Irfan Ullah is a Research Fellow in the Smart Electronics and Material Group, School of Electronics and Computer Science at the University of Southampton, UK. He obtained his B.Eng. degree in Electronic and Communications Engineering in 2016 and PhD degree in Electronic Engineering in 2020 from the University of Kent, UK. His current research interests include passive UHF RFID tags, small antennas, wireless power transfer and smart bandages for healthcare applications.

Alex S. Weddell (GS'06-M'10) received the M.Eng. degree (1st class honors) and Ph.D. in electronic engineering from the University of Southampton, U.K., in 2005 and 2010.

His main research focus is in the areas of energy harvesting and energy management for future Internet of Things devices. He has over 14 years of experience in the design and deployment of energy harvesting systems.He is currently a Lecturer in the Center for Internet of Things and Pervasive Systems, and is involved with projects funded by EPSRC, EU Horizon 2020 and Clean Sky 2.

Steve Beeby (FIEEE) received the B.Eng. (Hons.) degree in mechanical engineering from the University of Portsmouth, Portsmouth, U.K., in 1992, and the Ph.D. degree in MEMS resonant sensors from the University of Southampton, U.K., in 1998.

He is currently the Director of the Centre for Flexible Electronics and E-Textiles at the University of Southampton. He is a co-founder of Perpetuum Ltd., Smart Fabric Inks Ltd., and D4 Technology Ltd. His current research interests focus on energy harvesting, e-textiles and the use of energy harvesting in wearable applications.

Prof. Beeby was the recipient of two prestigious EPSRC Research Fellowships to investigate the combination of screen-printed active materials with micromachined structures and textiles for energy harvesting. He has most recently been awarded a prestigious RAEng Chair in Emerging Technologies in E-textile Engineering.